01 Jan 2005

Structure, Magnetic, and Transport Properties of Ti-substituted $La_{0.7}Sr_{0.3}MnO_3$

M. S. Kim

Jinbo Yang

Qingsheng Cai

X.-D. Zhou
Missouri University of Science and Technology

et. al. For a complete list of authors, see https://scholarsmine.mst.edu/matsci_eng_facwork/1481

Recommended Citation

M. S. Kim et al., "Structure, Magnetic, and Transport Properties of Ti-substituted $La_{0.7}Sr_{0.3}MnO_3$," *Physical Review B - Condensed Matter and Materials Physics*, vol. 71, no. 1, pp. 14433-14441, American Physical Society (APS), Jan 2005.
The definitive version is available at https://doi.org/10.1103/PhysRevB.71.014433

Structure, magnetic, and transport properties of Ti-substituted $La_{0.7}Sr_{0.3}MnO_3$

M. S. Kim,[1,2] J. B. Yang,[1,2] Q. Cai,[3] X. D. Zhou,[2] W. J. James,[2,4] W. B. Yelon,[2,4] P. E. Parris,[1] D. Buddhikot,[5] and S. K. Malik[5]

[1]*Department of Physics, University of Missouri-Rolla, Rolla, Missouri 65409, USA*
[2]*Graduate Center for Materials Research, University of Missouri-Rolla, Rolla, Missouri 65409, USA*
[3]*Department of Physics, University of Missouri-Columbia, Columbia, Missouri 65211, USA*
[4]*Department of Chemistry, University of Missouri-Rolla, Rolla, Missouri 65409, USA*
[5]*Tata Institute of Fundamental Research, Colaba, Mumbai 400-005, India*

(Received 19 July 2004; published 26 January 2005)

Ti-substituted perovskites $La_{0.7}Sr_{0.3}Mn_{1-x}Ti_xO_3$ with $0 \leqslant x \leqslant 0.20$, were investigated by neutron diffraction, magnetization, electric resistivity, and magnetoresistance (MR) measurements. All samples show a rhombohedral structure (space group $R\bar{3}c$) from 10 K to room temperature. At room temperature, the cell parameters a, c and the unit cell volume increase with increasing Ti content. However, at 10 K, the cell parameter a has a maximum value for $x=0.10$, and decreases for $x>0.10$, while the unit cell volume remains nearly constant for $x>0.10$. The average (Mn,Ti)-O bond length increases up to $x=0.15$, and the (Mn,Ti)-O-(Mn,Ti) bond angle decreases with increasing Ti content to its minimum value at $x=0.15$ at room temperature. Below the Curie temperature T_C, the resistance exhibits metallic behavior for the $x \leqslant 0.05$ samples. A metal (semiconductor) to insulator transition is observed for the $x \geqslant 0.10$ samples. A peak in resistivity appears below T_C for all samples, and shifts to a lower temperature as x increases. The substitution of Mn by Ti decreases the $2p$-$3d$ hybridization between O and Mn ions, reduces the bandwidth W, and increases the electron-phonon coupling. Therefore, the T_C shifts to a lower temperature and the resistivity increases with increasing Ti content. A field-induced shift of the resistivity maximum occurs at $x \leqslant 0.10$. The separation of T_C and the resistivity maximum temperature $T_{\rho,\max}$ enhances the MR effect in these compounds due to the weak coupling between the magnetic ordering and the resistivity as compared with $La_{0.7}Sr_{0.3}MnO_3$.

DOI: 10.1103/PhysRevB.71.014433 PACS number(s): 75.50.−y, 75.47.−m, 61.12.Ld, 61.10.−i

I. INTRODUCTION

The $A_{1-x}A'_xMnO_3$ perovskites are interesting systems because of the anomalous magnetic and transport properties exhibited by them such as colossal magnetoresistance (CMR), metal-insulator transitions, antiferromagnetic-ferromagnetic ordering, and lattice dynamics associated with phase transitions.[1–8] Zener's double exchange (DE) interaction between Mn^{3+} and Mn^{4+} ions through charge carriers in the oxygen $2p$ orbitals was introduced in order to explain the coupling of magnetic and electronic properties in these compounds.[9–12] Undoped $LaMnO_3$ is an A-type antiferromagnetic insulator. By substitution of La^{3+} with a divalent cation, $LaMnO_3$ can be driven into a metallic and ferromagnetic state. Both Mn^{3+} and Mn^{4+} ions possess a local spin ($S=3/2$) from their lower t_{2g}^3 orbitals, and Mn^{3+} has an extra electron in the e_g orbital which is responsible for conduction. The spin of the e_g^1 electron in Mn^{3+} is ferromagnetically coupled to the local spin of t_{2g}^3 according to Hund's rule. Sr doping induces holes in the e_g band near the Fermi energy, producing mobile holes and conduction. However, recent studies have shown that DE is not sufficient to explain the complex physics in these compounds, especially with regard to the lattice distortions coinciding with the emergence of CMR.[13,14] An understanding of the Sr-doped systems requires one to consider both DE interactions in the Mn^{3+}-O-Mn^{4+} pairs and the strong electron-phonon coupling, including lattice polarons and dynamic Jahn-Teller (JT) distortions.[15,16] The polaron effect arising from JT distortion was introduced to explain the electronic transport mechanism in the high-temperature region $T \approx T_C$, where a strong electron-phonon interaction is required to reduce the kinetic energy of the conduction electrons. The local JT distortion of the MnO_6 octahedron lowers the energy of the e_g^1 electron and the charge carrier can then be localized to form a lattice phonon. Therefore local lattice distortion above T_C rapidly decreases electron hopping, thus increasing the resistivity.[14] Recently, it was found that polaron hopping was also the dominant conduction mechanism below T_C.[17–20] A sharp increase of polaron density at temperatures below T_C leads to a charge carrier density collapse, which is related to the resistivity peak and the CMR of doped manganites.[21]

In order to understand the unusual magnetic and transport properties of doped perovskites $A_{1-x}D_xMnO_3$, many studies have been carried out by doping the trivalent rare earth site (A site) with divalent atoms (Ca, Sr, Ba, etc).[5,22–26] Other studies have also shown that substitution for Mn (B site) dramatically affects the magnetic and transport properties of perovskites.[27–30] The B site modification has merit in that it directly affects the Mn network by changing the Mn^{3+}/Mn^{4+} ratio and the electron carrier density. Therefore in order to better understand the role of Mn and its local environment in $La_{0.7}Sr_{0.3}MnO_3$, we studied the effects of replacing some of the Mn with Ti. The structural, magnetic and electrical phase transitions and transport properties of $La_{0.7}Sr_{0.3}Mn_{1-x}Ti_xO_3$ with $0 \leqslant x \leqslant 0.20$ have been investigated by neutron diffraction, magnetization, electric resistivity, and magnetoresistance measurements and the results are presented here.

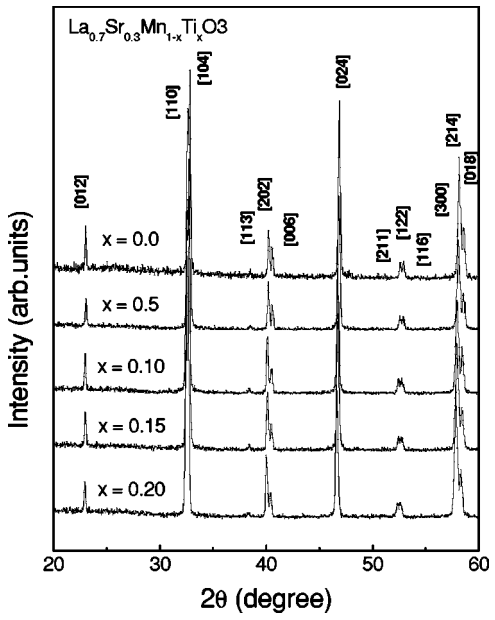

FIG. 1. X-ray diffraction patterns of $La_{0.7}Sr_{0.3}Mn_{1-x}Ti_xO_3$ ($0 \leqslant x \leqslant 0.20$) at room temperature.

II. EXPERIMENTAL

Samples of Ti-substituted $La_{0.7}Sr_{0.3}Mn_{1-x}Ti_xO_3$, with $0 \leqslant x \leqslant 0.2$, were prepared using the conventional solid state reaction method. Highly purified La_2O_3, $SrCO_3$, TiO_2, MnO were mixed in stoichiometric ratios, ground, and then pelletized under 3000 psi pressure to a 1 cm diameter. The pelletized samples were fired at 1500 °C in air for 12 h, then reground and sintered at 1250 °C for 24 h in air. X-ray diffraction of the powders was carried out at room temperature using a SCINTAG diffractometer with Cu-$K\alpha$ radiation. X-ray diffraction data indicated all samples to be single phase. Powder neutron diffraction experiments were performed at the University of Missouri–Columbia Research Reactor (MURR) using neutrons of wavelength $\lambda = 1.4875$ Å. The data for each sample were collected between $2\theta = 5.65 - 105.60°$ at 300 and 10 K. Refinement of the neutron diffraction data was carried out using the FULLPROF program,[31] which permits multiple phase refinements as well as magnetic structure refinements. Magnetic measurements were conducted with a SQUID magnetometer (MPMS, Quantum design). The magnetization curves with zero-field cooling (ZFC) and field cooling (FC) were measured in an applied magnetic field of 50 Oe. Resistivity data were obtained using a physical properties measurement system (PPMS, Quantum design) with a standard four-point probe method.

III. RESULTS AND DISCUSSION

Figure 1 shows the x-ray diffraction patterns of $La_{0.7}Sr_{0.3}Mn_{1-x}Ti_xO_3$ samples, with $0 \leqslant x \leqslant 0.2$, at room temperature (RT). All the samples are single phase and all peak positions can be indexed to $La_{0.67}Sr_{0.33}MnO_{2.91}$ (JCPDS 50-0308), space group $R\bar{3}c$. In order to investigate the details of the structural distortion and the magnetic interactions in these compounds, powder neutron diffraction measurements were performed at different temperatures. Figure 2 shows the neutron diffraction patterns of $La_{0.7}Sr_{0.3}Mn_{1-x}Ti_xO_3$ with $x = 0.0$, $x = 0.03$ and 0.20 measured at RT and 10 K. All patterns can be fitted with the $R\bar{3}c$ rhombohedral space group (No. 167) in which the atomic positions are La(Sr): $6a(0,0,1/4)$, Mn(Ti): $6b(0,0,0)$; O18$e(x,0,1/4)$. The $P1$ space group was used to fit the magnetic structure with collinear Mn magnetic moments because of its flexibility. Refined structural and magnetic parameters are listed in Tables I and II for RT and 10 K, respectively. For samples with $x \geqslant 0.10$, there is no magnetic ordering at RT since $T_C < RT$, whereas for samples with $x \leqslant 0.10$, $T_C > RT$ magnetic ordering is observed. The arrows on the neutron-diffraction patterns of the $x = 0.0$ sample (Fig. 2) indicate magnetic reflec-

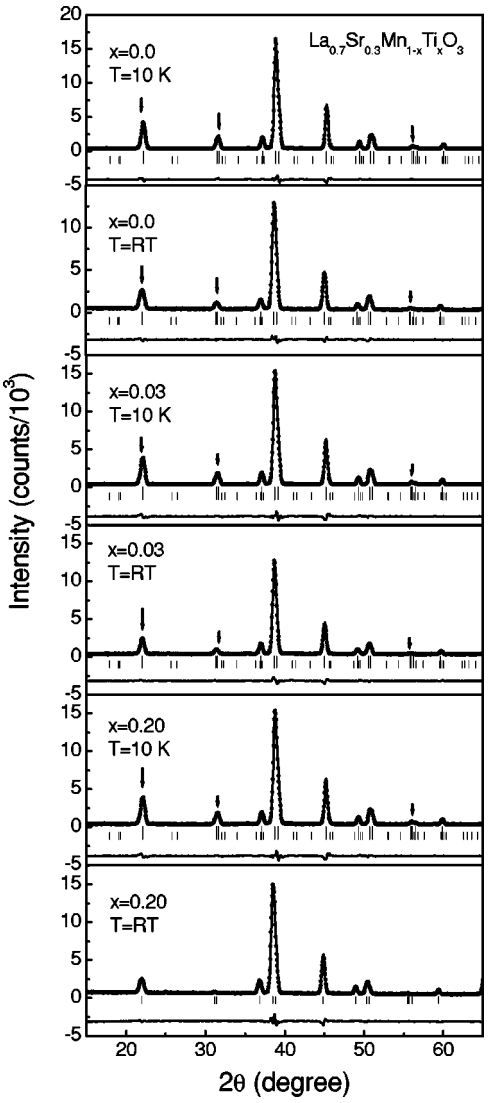

FIG. 2. Neutron-diffraction patterns of $La_{0.7}Sr_{0.3}Mn_{1-x}Ti_xO_3$ ($x = 0.0$, 0.03, and 0.20) at 10 K and RT. [The bottom curves (Y_{obs}-Y_{cal}) are the difference between experimental data and refinement data. The vertical bars indicate the magnetic (bottom) and Bragg (top) peak positions.] Arrows indicate some of major magnetic diffraction peaks.

TABLE I. Refined parameters for $La_{0.7}Sr_{0.3}Mn_{1-x}Ti_xO_3$ compound with $R\bar{3}c$ space group at room temperature ($T=300$ K). Numbers in parentheses are statistical errors. a and c are the lattice parameters. m is magnetic moment. V is the unit cell volume. B is the isotropic temperature parameter. χ^2 is $[R_{wp}/R_{\exp}]^2$ where R_{wp} is the residual error of the weighted profile.

Composition	0.00	0.03	0.05	0.10	0.15	0.20
a(Å)	5.5038(2)	5.5107(1)	5.5157(2)	5.5225(2)	5.5306(2)	5.5310(2)
c(Å)	13.3553(5)	13.3635(4)	13.3699(5)	13.3845(5)	13.4032(6)	13.4124(6)
V(Å^3)	350.364(18)	351.445(16)	352.261(18)	353.508(21)	355.042(22)	355.341(23)
$m(\mu_B)$	2.514(28)	2.121(33)	1.022(63)	0.0	0.0	0.0
χ^2(%)	2.81	3.28	3.60	3.23	4.64	2.98
O, 18e,x	0.5422(2)	0.5437(2)	0.5448(2)	0.5460(2)	0.5469(2)	0.5461(2)
B(Å^2), La(Sr), 6a	0.882(33)	0.8124(33)	0.873(35)	1.030(42)	0.975(43)	1.149(40)
B(Å^2), Mn(Ti), 6b	0.423(54)	0.556(56)	0.574(59)	0.364(66)	0.394(67)	0.404(63)
B(Å^2), O, 18e	1.221(25)	1.248(25)	1.306(27)	1.501(37)	1.475(37)	1.586(35)

tion peaks that are not present for the $x=0.20$ sample at RT. The peak intensities of the magnetic reflections decrease with Ti substitution at both RT and 10 K. In addition, the refinement results confirm that the substituted Ti ions go into B sites, not into A sites, because the ionic radius of Ti^{4+} (0.605 Å) lies between the ionic radius of Mn^{4+} (0.530 Å) and Mn^{3+} (0.645 Å).[32] The tolerance factor, which is the geometric measure of size mismatch of perovskites

$$t = (r_{(\mathrm{La,Sr})} + r_{\mathrm{O}})/[(r_{(\mathrm{Mn,Ti})} + r_{\mathrm{O}})\sqrt{2}] \quad (1)$$

decreases linearly from 0.928 for $La_{0.7}Sr_{0.3}MnO_3$ to 0.921 for $La_{0.7}Sr_{0.3}Mn_{0.8}Ti_{0.2}O_3$, which is in the stable range of the perovskite structure $0.89<t<1.02$.[26] Therefore, substitution of Mn by Ti does not change the crystal structure itself but changes the bond lengths and the bond angles of the MnO_6 octahedra.

Figure 3 plots the lattice parameters a,c and the unit cell volumes of $La_{0.7}Sr_{0.3}Mn_{1-x}Ti_xO_3$ versus the Ti(Ti^{4+}) content at room temperature and 10 K. The lattice parameters a,c and the unit cell volume increase with the Ti content at RT. At 10 K, the lattice parameter a shows a maximum value at $x=0.10$ and then decreases as $x>0.10$, and the unit cell volume increases up to $x=0.10$ and becomes almost constant for $x>0.10$. The refined magnetic moments of the Mn atoms indicate that Mn atoms have a high spin state, and the average valence state of the Mn varies from $3d^{3.5}$ to $3d^{3.3}$ for $x=0.0$ and $x=0.15$, which suggests that the Ti atoms are in the Ti^{4+} state. The values of the temperature factor B of oxygen increase with increasing Ti content which is consistent with the increase of the Mn-O bond length. This is likely related to the structural disorder in the position of oxygen atoms due to the substitution of Mn for Ti.

The average (Mn,Ti)-O bond length and (Mn,Ti)-O-(Mn,Ti) bond angle extracted from the Rietveld refinement at RT and 10 K are shown in Fig. 4. The bond length of $La_{0.7}Sr_{0.3}Mn_{1-x}Ti_xO_3$ increases up to $x=0.15$ and remains constant thereafter for $x\geqslant 0.15$, while the bond angle decreases and attains an anomalous minimum value for $x=0.15$ at RT. At 10 K, the bond length increases up to $x=0.10$ and remains constant for $x>0.10$, while the bond angle decreases with increasing x. The bond length and the bond angle are closely related to the oxygen positions.

TABLE II. Refined parameters for $La_{0.7}Sr_{0.3}Mn_{1-x}Ti_xO_3$ compound with the $R\bar{3}c$ space group at low temperature ($T=10$ K). Numbers in parentheses are statistical errors. a and c are the lattice parameters. m is magnetic moment. V is the unit cell volume. B is the isotropic temperature parameter. χ^2 is $[R_{wp}/R_{\exp}]^2$ where R_{wp} is the residual error of the weighted profile.

Composition	0.00	0.03	0.05	0.10	0.15	0.20
a(Å)	5.4811(1)	5.4940(1)	5.4989(1)	5.5116(1)	5.5089(2)	5.5053(3)
c(Å)	13.2756(3)	13.3037(4)	13.3137(4)	13.3354(4)	13.3421(6)	13.3746(10)
V(Å^3)	345.397(13)	347.756(14)	348.644(16)	350.820(15)	350.652(22)	351.056(35)
$m(\mu_B)$	3.443(25)	3.461(27)	3.506(32)	3.422(28)	3.282(36)	2.913(51)
χ^2(%)	3.23	3.51	2.89	2.69	3.72	4.90
O, 18e,x	0.5431(1)	0.5442(2)	0.5448(1)	0.5467(1)	0.5469(2)	0.5472(2)
B(Å^2), La(Sr), 6a	0.167(26)	0.240(28)	0.302(33)	0.318(28)	0.449(37)	0.269(48)
B(Å^2), Mn(Ti), 6b	0.127(45)	0.230(49)	0.271(57)	0.169(47)	0.291(62)	0.174(81)
B(Å^2), O, 18e	0.328(21)	0.536(23)	0.595(27)	0.649(22)	0.926(28)	0.945(36)

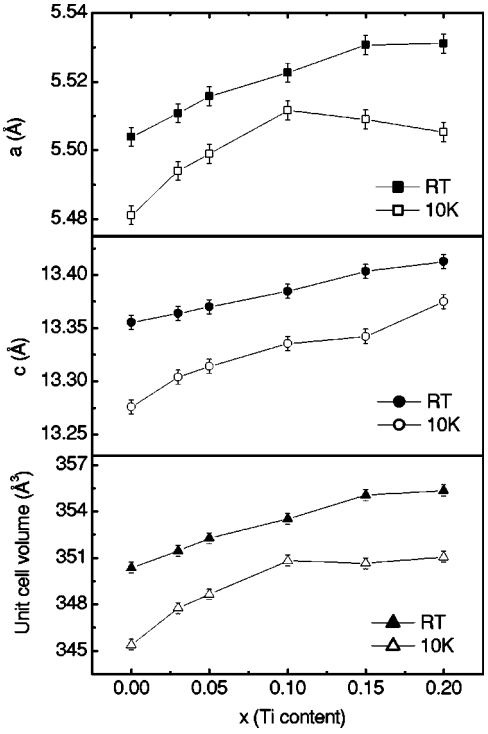

FIG. 3. Lattice parameter a,c, and volume of $La_{0.7}Sr_{0.3}Mn_{1-x}Ti_xO_3$ versus Ti content at room temperature and at 10 K.

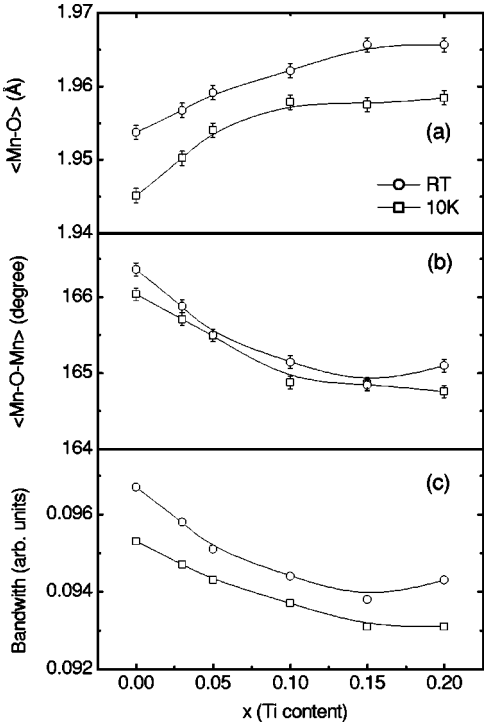

FIG. 4. Average (Mn,Ti)-O bond lengths (a), (Mn,Ti)-O-(Mn,Ti) bond angles (b), and electronic bandwidth parameter $\cos\omega/(d_{\text{Mn-O}})^{3.5}$ (c) of $La_{0.7}Sr_{0.3}Mn_{1-x}Ti_xO_3$ at room temperature and at 10 K.

Therefore, an increasing (Mn-Ti)-O bond length and a decreasing (Mn,Ti)-O-(Mn,Ti) bond angle are strongly correlated. The changes in bond length and bond angle of MnO_6 compensate one another to diminish the internal strain induced by Ti^{4+}. Since the exchange interaction between Mn-Mn depends on both the bond angle and the bond distance, the decrease in bond angle and the increase in bond length decrease the Mn-Mn exchange interaction which leads to a lower magnetic ordering temperature T_C (see later discussion of M-T curves).

The electronic bandwidth W has been used to discuss magnetic and transport properties of perovskites with varied A-site doping.[16,33] The empirical formula of the bandwidth W for ABO_3-type perovskites using the tight binding approximation[24] is

$$W \propto \frac{\cos\omega}{(d_{\text{Mn-O}})^{3.5}}, \tag{2}$$

where $\omega=\frac{1}{2}(\pi-\langle\text{Mn-O-Mn}\rangle)$ and $d_{\text{Mn-O}}$ is the Mn-O bond length. The calculated values of $\cos\omega/(d_{\text{Mn-O}})^{3.5}$ using the refinement results are shown in Fig. 4(c). We assumed the bandwidth W is proportional to the values of $\cos\omega/(d_{\text{Mn-O}})^{3.5}$. It is found that the bandwidth W decreases with increasing Ti content. Further, the bandwidth at RT is smaller than the bandwidth at 10 K for a given Ti content. The evolution of the bandwidth follows the change in the $\langle$Mn-O-Mn$\rangle$ bond angle. The decrease in bandwidth reduces the overlap between the O-2p and the Mn-3d orbitals, which in turn decreases the exchange coupling of Mn^{3+}-Mn^{4+}, and the magnetic ordering temperature T_C as well. For a charge-transfer insulator, the band gap energy E_g in the insulating phase can be written as $E_g=\Delta-W$, where Δ is the charge-transfer energy and W is the O-2p-like bandwidth. In practice, Δ changes little in the $La_{1-x}Sr_xMnO_3$ system and thus the bandwidth W becomes a main factor in tuning the band gap energy.[34] For the $La_{0.7}Sr_{0.3}Mn_{1-x}Ti_xO_3$ compounds, the decrease in bandwidth W increases the band gap E_g and leads to the metal to insulator transition for $x>0.10$.

Figure 5 shows the magnetization versus temperature (M-T) curves measured under field-cooled (FC) and zero field-cooled (ZFC) conditions in a magnetic field of 50 Oe for the $x=0.05$, 0.10, and 0.15 samples. A sharp paramag-

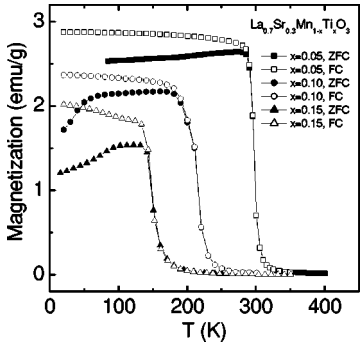

FIG. 5. The magnetization versus temperature (M-T) curves of $La_{0.7}Sr_{0.3}Mn_{1-x}Ti_xO_3$ ($x=0.05,0.10,0.15$) measured under field cooling (FC) and zero field cooling (ZFC) conditions in a magnetic field of 50 Oe.

netic to ferromagnetic transition is observed at a critical temperature T_C. Figure 6 shows the Curie temperatures T_C of $La_{0.7}Sr_{0.3}Mn_{1-x}Ti_xO_3$ for differing Ti content. The decrease in T_C is obviously related to the changes in bandwidth as seen in Fig. 4(c). The T_C drops at a rate of about 10 K per Ti. λ-shaped magnetization curves in ZFC emerge for $x \geqslant 0.10$ samples. The existence of λ-shaped curves under ZFC may be evidence of the formation of ferromagnetic clusters with a spin glass state. The Ti substitution weakens the exchange interaction and breaks the Mn-O-Mn network, and creates short range ordered ferromagnetic clusters. As more Ti is substituted, more inhomogeneous clusters are formed, which leads to a broadening of the paramagnetic to ferromagnetic phase transition peak. A similar phenomenon has been observed in the $La_{0.7}Ca_{0.3}Mn_{1-x}Ti_xO_3$ system.[26]

Magnetization versus field (M-H) curves of $La_{0.7}Sr_{0.3}Mn_{1-x}Ti_xO_3$ at different temperatures are plotted in Fig. 7. At 20 K, all samples reach a nearly constant value of magnetization under a field $H=0.6$ T. The estimated magnetic moments of the $x=0.0$, 0.05, 0.10, and 0.15 samples from magnetization data at 20 K are 3.79, 3.54, 3.24, and 2.49 μ_B per Mn atom, respectively. These moment values are in good agreement with the neutron diffraction refinement results (see Table II). The theoretically estimated magnetic moments of Mn from its valence state taking into account the dilution effect of Ti^{4+}, are 3.70, 3.55, 3.40, and 3.35 μ_B, respectively. This suggests that the decrease of magnetization with increasing Ti content is not only due to the dilution of magnetic Mn^{4+} atoms but also due to the weakening of exchange coupling by the cluster formation.

Figure 8 shows the resistivity as a function of temperature under different applied fields for $La_{0.7}Sr_{0.3}Mn_{1-x}Ti_xO_3$ compounds with $x=0.0$, 0.05, 0.10, and 0.15. In the temperature range 4–300 K, the resistivity of the samples increases as the Ti content increases. The resistivity of $0.05 \leqslant x \leqslant 0.10$ shows a maximum value at temperature $T_{\rho,\max}$ below T_C, and then decreases as the temperature decreases. Finally the resistivity increases again as T decreases further for $x \geqslant 0.10$. The difference between T_C and $T_{\rho,\max}$ becomes larger as the Ti content increases and $T_{\rho,\max}$ is lower than T_C. This behavior is quite different from that observed in the Ti-substituted $La_{0.7}Ca_{0.3}Mn_{1-x}Ti_xO_3$ series which exhibit large differences between T_C and $T_{\rho,\max}$ (Ref. 25) and $T_{\rho,\max}$ is higher than T_C.[26] For the $x \leqslant 0.15$ sample, a metal (semiconductor) to insulator transition (MIT) appears in the low-temperature region. The field-induced shift of maximum resistivity to higher temperature appears for the $x \leqslant 0.10$ samples, and becomes negligible for $x \geqslant 0.15$. The suppression of the resistivity by the applied magnetic field occurs over the entire temperature range for all samples. At $T > T_C$, the suppression of the resistivity becomes weaker. According to the DE mechanism, the mobility of the charge carriers e_g electrons improves if the localized spins are polarized. The applied field aligns the canted electron spins which should reduce the scattering of itinerant electrons with spins and thus the resistivity is reduced. Therefore an applied magnetic field competes with the thermal fluctuations and maintains magnetic ordering around T_C for the $x \leqslant 0.10$ samples, and thus shifts the $T_{\rho,\max}$ to higher temperatures.

Figure 9 shows the typical temperature dependence of the magnetoresistance $[MR=(\rho_0-\rho_H)/\rho_0 \times 100]$ of $La_{0.7}Sr_{0.3}Mn_{1-x}Ti_xO_3$ samples with $0 \leqslant x \leqslant 0.20$ under an applied field of 1 and 3 T. The maximum magnetoresistance increases with increasing Ti concentration. For example, the maximum MR values are 30, 55 % under 3 T for $x=0.05$, 0.15, respectively. The temperature of the MR peak shifts to a lower temperature, approximately 15 K per Ti. It is known that in A-site electron-doped $A_{1-x}A'_xMnO_3 (x=0.3)$ compounds, the metal-insulator transition temperature T_{MI} coincides with the T_C, and the metal-insulator transition is strongly coupled with the magnetic ordering transition. Therefore, a strong variation of the electrical resistivity up to several orders of magnitude, namely, the colossal magnetoresistance (CMR) effect, occurs upon application of a magnetic field near T_C. However, for $La_{0.7}Sr_{0.3}Mn_{1-x}Ti_xO_3$ compounds, the T_C is different than from the metal to insulator transition temperature. The application of a magnetic field has much more effect on the change of electric resistivity when compared to $La_{0.7}Sr_{0.3}MnO_3$ due to the weak coupling between the MIT and the magnetic ordering. An enhancement of the MR effect is observed in these compounds, similar to that in $La_{0.7}Ca_{0.3}Mn_{1-x}Ti_xO_3$ (Refs. 25 and 26) and $Pr_{1-x}(Ca,Sr)_xMnO_3$ compounds.[35]

The change of the electronic properties of Ti-substituted $La_{0.7}Ca_{0.3}Mn_{1-x}Ti_xO_3$ compounds is strongly related to the electron phonon coupling.[14] Accordingly, in the $La_{1-x}Sr_xMnO_3$ system, the strong electron-phonon coupling localizes the conduction band electron as a polaron, due to

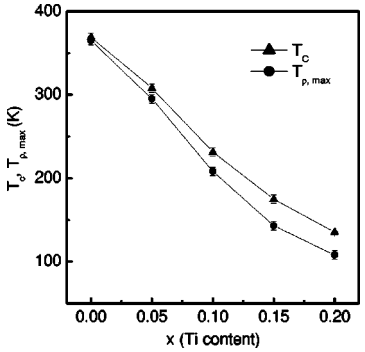

FIG. 6. The Curie temperature (T_C), and the temperature of maximum resistivity ($T_{\rho,\max}$) of $La_{0.7}Sr_{0.3}Mn_{1-x}Ti_xO_3$ compounds with $0 \leqslant x \leqslant 0.20$.

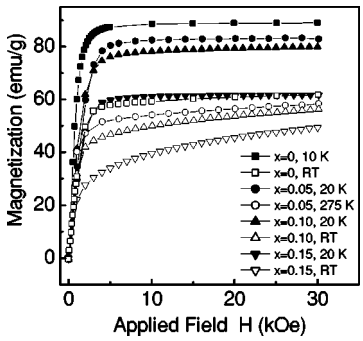

FIG. 7. Field-dependent magnetization of $La_{0.7}Sr_{0.3}Mn_{1-x}Ti_xO_3$ ($0 \leqslant x \leqslant 0.20$) at different temperatures.

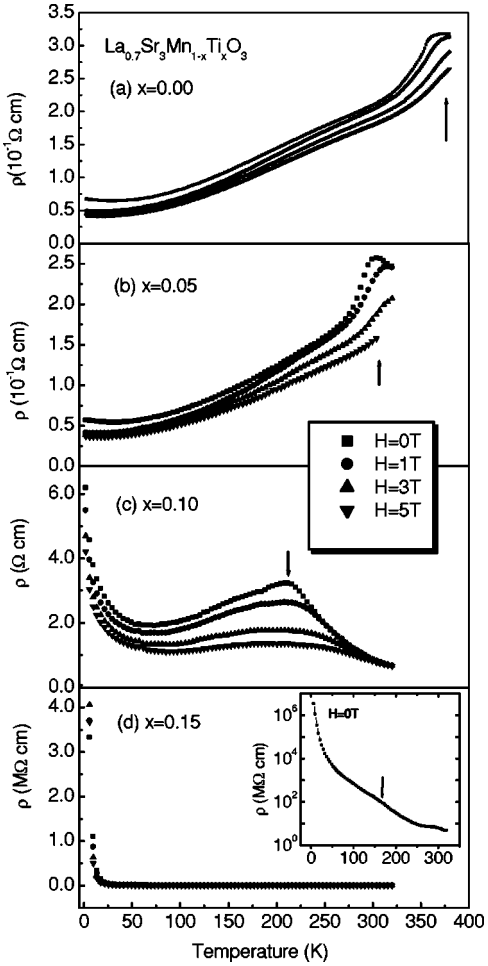

FIG. 8. Electric resistivity ρ versus temperature for $La_{0.7}Sr_{0.3}Mn_{1-x}Ti_xO_3$ compounds [$x=0.0$ (a), 0.05 (b), 0.10 (c), and 0.15 (d)] in applied magnetic field $H=0$, 1, 3, and 5 T. Arrows indicate the $T_{\rho,\max}$. The inset in (d) is the plot of resistivity of $x=0.15$ compound (with log scale) in $H=0$ T.

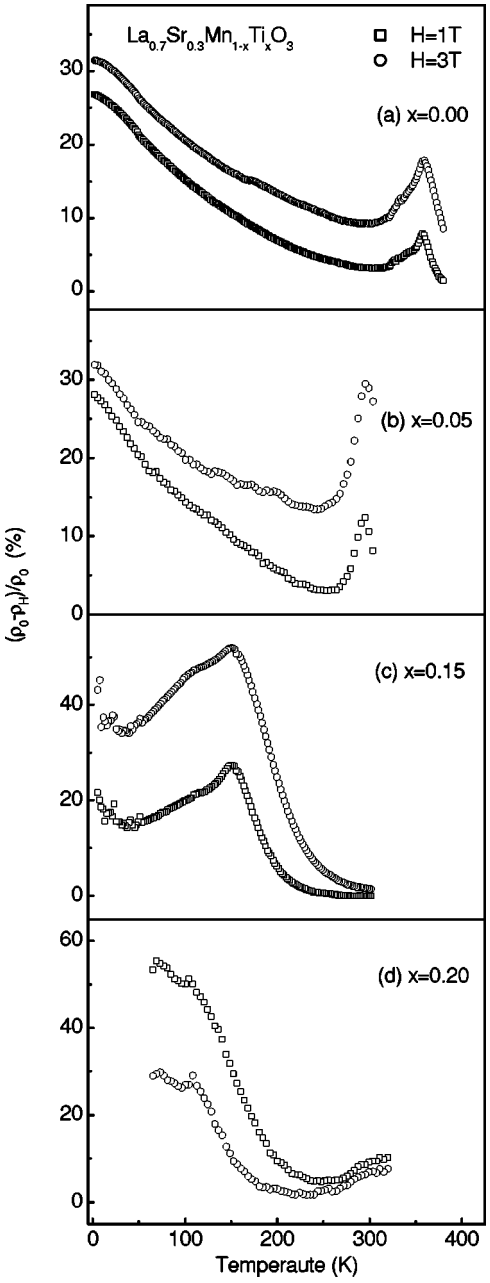

FIG. 9. Temperature dependence of magnetoresistance of $La_{0.7}Sr_{0.3}Mn_{1-x}Ti_xO_3$ ($0\leqslant x\leqslant 0.20$) compounds in the magnetic field of $H=1,3$ T.

the competition between the self-trapping energy $E_{J,T}$ and the electron itinerant energy. The electron-phonon coupling constant $\lambda=E_{J,T}/t$, where t is the electron hopping parameter which is proportional to the electronic bandwidth W. As mentioned above, the substitution of Mn by Ti decreases the overlap of the O-2p and Mn-3d orbitals due to the decrease in W, thus increasing the electron-phonon coupling. This results in a shift of T_C to lower temperatures and an increase of resistivity with increasing Ti content. As a consequence, one should consider a possible dependence of $E_{J,T}$ on Ti content. We cannot rule out the contribution from $E_{J,T}$, even though our data indicate that all the observed T_C and resistivity changes can be explained, at least qualitatively, by the change in W. Especially, for $x\geqslant 0.15$, the electron-phonon coupling becomes very strong, and the insulator behavior occurs below T_C as shown in Fig. 8. The changes in bandwidth W are not large enough to account for the dramatic changes in resistivity, and therefore, $E_{J,T}$ might be contributing significantly to the change of resistivity in these samples.

It has been proposed that, above T_C, charge may be localized in the form of JT polarons.[21] At $T\geqslant T_C$, the resistivity of the CMR materials can be explained by the activated adiabatic polaron equation[36]

$$\rho = AT\exp(E_{\mathrm{hop}}/kT). \tag{3}$$

Figure 10 shows the plot of $\ln(\rho/T)$ as a function of $1/T$ for $La_{0.7}Sr_{0.3}Mn_{1-x}Ti_xO_3$ compounds with $x=0.00$, 0.05, 0.10, 0.15, and 0.20 in the high-temperature region with zero field resistivity data. Resistivity of all the samples shows a similar slope at $T\geqslant T_C$, which can be fitted well with the small polaron model indicating the formation of a polaron. The polaron hopping energy E_{hop} is calculated from the slopes. The calculated values of E_{hop} are 14.5 49.8, 132.0,

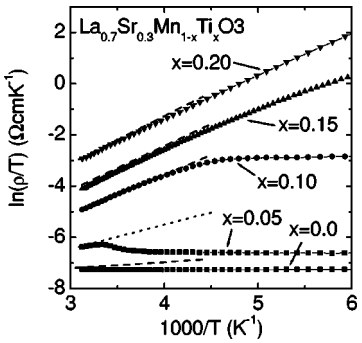

FIG. 10. $\ln(\rho/T)$ versus $1/T$ plots in the high-temperature region of $La_{0.7}Sr_{0.3}Mn_{1-x}Ti_xO_3$ ($0 \leqslant x \leqslant 0.20$) compounds. The dotted line is the fitting line.

138.3, and 152.5 meV for $x=0.00$, 0.05, 0.10, 0.15, and 0.20, respectively. The increase of E_{hop} is due to the substitution of Mn by Ti which depletes the oxygen p holes and leads to an increase in the polaron binding energy. This further confirms that Ti substitution at Mn enhances the electron-phonon interaction, which decreases W and increases E_{hop} at high temperatures. The calculated polaron hopping energy shows a large variation between the $x=0.05$ and the $x \geqslant 0.10$ samples. This is in good agreement with the sharp increase in resistivity and its temperature dependence. Some studies have also suggested that polaron hopping is the prevalent mechanism to explain resistivity below T_C.[37–39] However, we were unable to fit the resistivity data of the Ti-doped $La_{0.7}Sr_{0.3}MnO_3$ samples below T_C with several other polaron models such as the semiconducting model,[40] the variable range hopping (VHR) polaron model,[41] and the adiabatic polaron hopping model. Only the VHR polaron model works reasonably well for the low temperature region $T<75$ K, for the insulating state, $x=0.10$ sample. There may be other contributions, such as ferromagnetic clusters, which would increase the resistivity of the compound.

IV. SUMMARY

The magnetic and electronic transport properties of Ti-substituted $La_{0.7}Sr_{0.3}Mn_{1-x}Ti_xO_3$ have been systematically investigated. All the Ti-substituted $La_{0.7}Sr_{0.3}Mn_{1-x}Ti_xO_3$ compositions have a rhombohedral structure (space group $R\bar{3}c$). The correlation between ferromagnetic T_C and $T_{\rho,\max}$ becomes weaker and spin glass clusters are expected in the low-temperature region with increasing Ti substitution. The resistivity in the high-temperature region suggests the formation of localized polarons that affect the strong correlation between local structural changes and the MIT. The decrease of the bandwidth W decreases the overlap between the O-2p and Mn-3d orbitals, which in turn decreases the exchange coupling of Mn-Mn and the magnetic ordering temperature T_c as well. Our studies indicate that Ti substitution at Mn enhances the electron-phonon interaction in these compounds, which decreases the bandwidth and increases the resistivities in the entire temperature range.

ACKNOWLEDGMENTS

The authors thank Aranwela Hemantha for invaluable help in magnetoresistance measurements. The support by DOE under DOE Contract No. DE-FC26-99FT400054 is acknowledged.

[1] C. W. Searle, S. T. Wang, Can. J. Phys. **47**, 2703 (1969).
[2] J. B. Goodenough, *Magnetism and the Chemical Bond* (Interscience, New-York, 1963).
[3] R. M. Kusters, J. Singleton, D. A. Keen, R. McGreevy, and W. Hayes, Physica B **155**, 362 (1989).
[4] R. von Helmolt, J. Wecker, B. Holzapfel, L. Schultz, and K. Samwer, Phys. Rev. Lett. **71**, 2331 (1993).
[5] S. Jin, T. H. Tiefel, M. McCormack, R. A. Fastnacht, R. Ramesh, and L. H. Chen, Science **264**, 413 (1994).
[6] A. Urushibara, Y. Moritomo, T. Arima, A. Asamitsu, G. Kido, and Y. Tokura, Phys. Rev. B **51**, 14103 (1995).
[7] Y. Tomioka, A. Asamitsu, H. Kuwahara, Y. Moritomo, and Y. Tokura, Phys. Rev. B **53**, R1689 (1996).
[8] Y. Tokura, in *Contribution to Colossal Magnetoresistance Oxides, Monographs in Condensed Matter Science*, edited by Y. Tokura (Gordon & Breach, London, 1999).
[9] C. Zener, Phys. Rev. **82**, 403 (1951).
[10] P. W. Anderson and H. Hasegawa, Phys. Rev. **100**, 675 (1955).
[11] P. G. de Gennes, Phys. Rev. **118**, 141 (1960).
[12] K. Kubo, N. Ohata, J. Phys. Soc. Jpn. **33**, 21 (1972).
[13] A. J. Millis, P. B. Littlewood, and B. I. Shraiman, Phys. Rev. Lett. **74**, 5144 (1995).
[14] A. J. Millis, B. I. Shraiman, and R. Mueller, Phys. Rev. Lett. **77**, 175 (1996).
[15] P. Dai, J. Zhang, H. A. Mook, S. H. Liou, P. A. Dowben, and E. W. Plummer, Phys. Rev. B **54**, R3694 (1996).
[16] P. G. Radaelli, G. Iannone, M. Marezio, H. Y. Hwang, S-W. Cheong, J. D. Jorgensen, and D. N. Argyriou, Phys. Rev. B **56**, 8265 (1997).
[17] H. L. Ju, H. C. Sohn, and K. M. Krishnan, Phys. Rev. Lett. **79**, 3230 (1997).
[18] D. S. Dessau, T. Saitoh, C. H. Park, Z. X. Shen, P. Villella, N. Hamada, Y. Moritomo, and Y. Tokura, Phys. Rev. Lett. **81**, 192 (1998).
[19] K. H. Kim, J. H. Jung, and T. W. Noh, Phys. Rev. Lett. **81**, 1517 (1998).
[20] G. M. Zhao, V. Smolyaninova, W. Prellier, and H. Keller, Phys. Rev. Lett. **84**, 6086 (2000).
[21] A. S. Alexandrov and A. M. Bratkovsky, Phys. Rev. Lett. **82**, 141 (1999).
[22] J. J. Neumeier, K. Andres, and K. J. McClellan, Phys. Rev. B **59**, 1701 (1999).
[23] M. Muroi, R. Street, and P. G. McComick, J. Appl. Phys. **87**, 3424 (2000).
[24] M. Medarde, J. Mesot, P. Lacorre, S. Rosenkranz, P. Fischer, and K. Gobrecht, Phys. Rev. B **52**, 9248 (1995).
[25] D. Cao, F. Bridges, M. Anderson, A. P. Ramirez, M. Olapinski, M. A. Subramanian, C. H. Booth, and G. H. Kwei, Phys. Rev. B

64, 184409 (2001).
[26] Xiaming Liu, Xiaojun Xu, and Yuheng Zhang, Phys. Rev. B **62**, 15112 (2000).
[27] C. Martin, A. Maignan, and B. Raveau, J. Mater. Chem. **6**, 1245 (1996).
[28] K. H. Ahn, X. W. Wu, K. Liu, and C. L. Chien, J. Appl. Phys. **81**, 5505 (1997).
[29] J. Blasco, J. Garcia, J. M. de Teresa, M. R. Ibarra, J. Perez, P. A. Algarabel, C. Marquina, and C. Ritter, Phys. Rev. B **55**, 8905 (1997).
[30] A. Mellergard, R. L. McGreevy, and S. G. Eriksson, J. Phys.: Condens. Matter **12**, 4975 (2000).
[31] J. Rodriguez-Carvajal, FULLPROF, Version 3.5d.
[32] R. D. Shannon, Acta Crystallogr., Sect. A: Cryst. Phys., Diffr., Theor. Gen. Crystallogr. **32**, 751 (1976).
[33] H. Y. Hwang, S-W. Cheong, P. G. Radaelli, M. Marezio, and B. Batlogg, Phys. Rev. Lett. **75**, 914 (1995).
[34] W. A. Harrison, *The Electronic Structure and Properties of Solids* (Freeman, San Francisco, 1980).
[35] A. Maignan, C. Martin, and B. Raveau, Z. Phys. B: Condens. Matter **102**, 19 (1997).
[36] D. Emin and T. Holstein, Ann. Phys. (N.Y.) **53**, 439 (1969).
[37] M. R. Ibarra, J. M. De Teresa, J. Blasco, P. A. Algarabel, C. Marquina, J. Garcia, J. Stankiewicz, and C. Ritter, Phys. Rev. B **56**, 8252 (1997).
[38] M. F. Hundley, M. Hawley, R. H. Heffner, Q. X. Jia, J. J. Neumeier, J. Tesmer, J. D. Thompson, and X. D. Wu, Appl. Phys. Lett. **67**, 860 (1995).
[39] W. E. Pickett and D. J. Singh, Phys. Rev. B **53**, 1146 (1996).
[40] N. F. Mott and E. A. Davis, *Electronics Processes in Noncrystalline Materials* (Clarendon, Oxford, 1971).
[41] Y. Sun, X. J. Xu, and Y. H. Zhang, J. Phys.: Condens. Matter **12**, 10 475 (2000).